論文 / 著書情報
Article / Book Information

Title	Push–Pull Bridged Distyrylbenzene with Highly Bright Solid-State Red-Orange Aggregation-Induced Emission
Authors	Yoshimichi Shimomura, Gen-ichi Konishi
Citation	Chemistry – A European Journal, Vol. 29, , e202301191
Pub. date	2023, 5
DOI	https://doi.org/10.1002/chem.202301191
Creative Commons	See next page.

License

Chemistry–A European Journal
Research Article
doi.org/10.1002/chem.202301191
Chemistry Europe
European Chemical Societies Publishing
www.chemeurj.org

Push-Pull Bridged Distyrylbenzene with Highly Bright Solid-State Red-Orange Aggregation-Induced Emission

Yoshimichi Shimomura[a] and Gen-ichi Konishi*[a]

Abstract: Multiple emission colors in solid-state organic fluorophores with the same main skeleton are essential for improving the performance of light-emitting devices/materials. Specifically, emission in the red/near-infrared region is of great importance in the biological field. Previously, we developed di-bridged-distyrylbenzene **DBDB[7]** with high-brightness solid-state blue and aggregation-induced emissions (AIE) by introducing the bridging structures of a seven-membered ring into the vinylene groups of distyrylbenzene (**DSB**). Herein, we synthesize **MNDBDMeODB[7]** (**1**), which features substituted methoxy and malononitrile groups as donor and acceptor groups, respectively, in **DBDB[7]**. In solvents more polar than THF, **MNDSDMeOB** (**3**), which has the same main skeleton as **1** but without bridges, shows no emission in the solid state, whereas **1** exhibits highly bright red-orange emission in the solid state owing to the suppression of intermolecular electronic interactions by the bridges and the AIE property. We also synthesize **MNDSD(EHO)B** (**2**) in which the methoxy groups of **3** are replaced by ethylhexyloxy groups, thus disrupting the crystallinity of the molecule. **2** exhibits positive fluorescence solvatochromism and has a high fluorescence quantum yield in the solid state as a red-emitting **DSB** derivative. The solid-state emission properties of **1** and **2** will improve the applicability of **DSB**s and functionalities of light-emitting devices/materials.

Introduction

Organic light-emitting materials, such as OLEDs,[1] bioimaging,[2] lasers,[3] security inks,[4] and high-sensitivity chemical sensors,[5] are widely used in the 21st century owing to their low cost, light weight, processability, versatility in molecular design, and no resource risks involving rare metals. However, to achieve higher performance and diversification, these devices require the development of high-performance advanced fluorescent dyes. An effective strategy to develop such dyes includes the synergistic effect of π-electron backbone and polar functional groups. A common luminescent π-conjugated molecule is *trans*-distyrylbenzene (**DSB**).[6] **DSB** is an oligo-phenylenevinylene molecule with a simple structure, three benzene rings, and easily introduced substituents. **DSB** exhibits high molar absorption and a high-emission quantum yield (Φ) in both the solution (0.89) and solid states (0.53).[7] Moreover, it has excellent properties that do not cause concentration quenching in the solid state, which usually occurs in the case of conventional fluorescent dyes.[8] Owing to the interesting features of **DSB**, many **DSB** derivatives substituted with various functional groups have been developed. These derivatives can be categorized into three groups: unsubstituted vinylene unit group,[6,9] methyl-substituted vinylene unit group,[10] and cyano-substituted vinylene unit group.[9,11] In particular, the cyano-substituted **DSB**s have been extensively investigated because their dyes form J-aggregates and exhibit strong emissions.

Meanwhile, for molecular imaging applications in biological and material sciences, balancing red emission and aggregation-induced emission (AIE) properties is important. The red/near-infrared emission range is considered as the so-called "biological window" because it shows high permeability in biological tissues and hence is used in high resolution imaging techniques.[12] AIE has been extensively studied[13–15] since Tang proposed[15] it as a quenching phenomenon in solution and as an emission property of the solid/aggregate states. The applications of AIE include the background-free analysis of living systems,[16] non-invasive treatments for cancer and other diseases,[17] and the design of highly efficient solid-state light-emitting materials.[18] Numerus studies related to **DSB** have been conducted, some of which report the solid-state red/near-infrared emission properties of **DBS**-based dyes.[19] However, (2Z,2′Z)-2,2′-(1,4-phenylene)bis(3-(4-(dibutylamino)phenyl)acrylonitrile), substituted cyano groups into the vinylene units, is known as one example of red-emitting AIE type **DSB** derivative.[20] Such a **DSB** dye emits light by forming J-aggregates. Because of the importance of red-emitting AIE luminogens (AIEgens), more AIE-type red-emitting **DSB** derivatives need to be developed. Monomeric luminescent AIEgens, which emit light in a physically adsorbed state, are particularly useful in molecular imaging. Moreover, to develop the crystal forms of organic light-emitting compounds with

[a] *Y. Shimomura, Prof. Dr. G.-i. Konishi*
Department of Chemical Science and Engineering
Tokyo Institute of Technology
2-12-1 O-okayama, Meguro-ku, Tokyo 152-8552 (Japan)
E-mail: konishi.g.aa@m.titech.ac.jp

Supporting information for this article is available on the WWW under https://doi.org/10.1002/chem.202301191

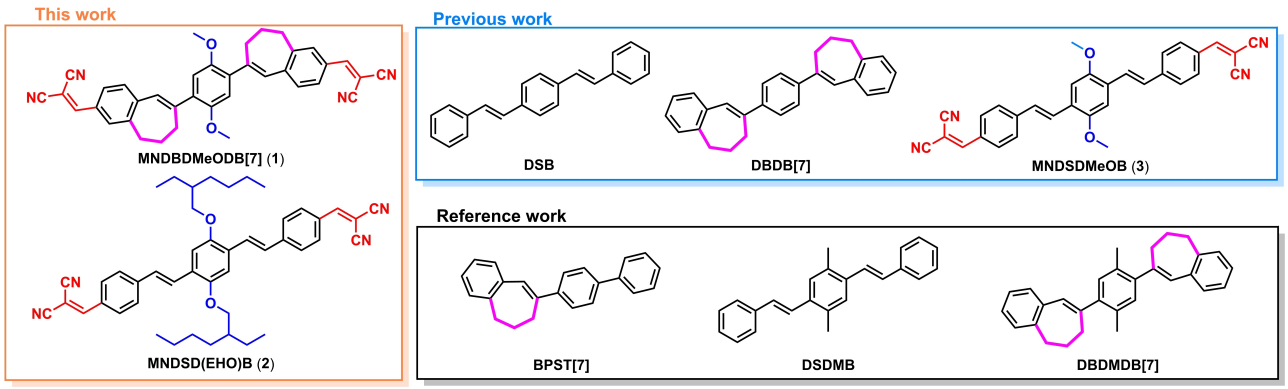

Figure 1. Chemical structures of previous and this works' compounds. **DSB**,[6] **DBDB[7]**,[7] **MNDSDMeOB**,[22] **BPST[7]**,[13] **DSDMB**,[7] **DBDMDB[7]**[7].

diverse functions, unsubstituted vinylene **DSB**s need to be developed.

Recently, we succeeded in providing **DSB** with AIE functions by introducing a bridging structure into the stilbene moiety, 1,4-bis(6,7-dihydro-5H-benzo[7]annulen-8-yl)benzene (di-bridged-**DSB**: **DBDB[7]**, Figure 1).[7] The bridging structure is a seven-membered ring in which a propylene group connects the vinyl group and outer benzene ring of **DSB**. This bridging structure increases the accessibility of the conical intersection (CI) of **DSB** with vinyl group cleavage in dilute solutions, which is common in stilbene-based molecules,[21] and promotes non-radiative decay from excited states. **DBDB[7]** exhibits high Φ with high dye density, unlike typical AIEgens, such as tetraphenylethene (**TPE**) and hexaphenylsilole (**HPS**).[15] In the solid/aggregate states, a singular conformation and steric hindrance decrease intermolecular electronic interactions, and **DBDB[7]** exhibits monomeric emission with high Φ. We hypothesized that a red-emitting-AIE **DSB** independent of J-aggregate formation could be designed by introducing a bridging structure into red-emitting **DSB**s with unsubstituted vinylene. We chose 2,2′-((((1E,1′E)-(2,5-dimethoxy-1,4-phenylene)bis(ethene-2,1-diyl))bis(4,1-phenylene))bis(methaneylylidene))dimalononitrile (**MNDSDMeOB** (**3**), Figure 1) as a model red-emitting **DSB**, which was reported by Li et al.[22] In the literature, **3** emits red color only in highly polar solvents and shows fluorescent solvatochromism.[22] However, its luminescence properties in the solid state have not been investigated. We synthesized **3** and investigated its photophysical properties in the solid state; **3** showed no emission. The fluorescence quenching of **3** in the solid state is due to the formation of H-aggregates.

In this study, we developed 2,2′-(((2,5-dimethoxy-1,4-phenylene)bis(6,7-dihydro-5H-benzoannulene-8,3-diyl))bis(methaneylylidene))dimalononitrile (**MNDBDMeODB[7]**) (**1**), which features bridging structures at the vinylene units of **3**, to prepare AIEgens that exhibit red emission in the solid state, and examined the photophysical properties of the resulting compound in the solution and solid states. We have shown that the introduction of the bridging structure into a vinylene unit is useful for designing AIEgens and achieving strong solid-state luminescence without using J-aggregate formation. Furthermore, we designed 2,2′-((((1E,1′E)-(2,5-bis((2- ethylhexyl)oxy)-1,4-phenylene)bis(ethene-2,1-diyl))bis(4,1-phenylene))bis-(methaneylylidene))dimalononitrile (**MNDSD(EHO)B**) (**2**), in which the ethylhexyloxy groups replace the methoxy groups of **3** with decreased crystallinity, and investigated its photophysical properties. **2** showed red fluorescence in both solution and the solid state. Thus, a non-luminescent **DSB** dye in the solid state could be transformed into a luminescent dye by introducing substituents that prevent the formation of crystals in the π-electron backbone.

Results and Discussion

We synthesized **1** using a scheme similar to that employed to obtain **DBDB[7]** (Scheme 1 and 2, see the Experimental Section). 6-Bromo-1-tetralone was used as the starting material, Br was transformed into a formyl group, and **1** was obtained via Knoevenagel condensation with malononitrile. **2** and **3** were obtained using the Mizoroki-Heck reaction and Knoevenagel condensation. (Scheme S1)

The photophysical properties of **1**, **2**, and **3** in toluene, chloroform ($CHCl_3$), tetrahydrofuran (THF), dichloromethane (CH_2Cl_2), dimethylformamide (DMF), their solid states, and 0.1 wt.% doped polymethylmethacrylate (PMMA; $M_n = 100$ k) cast films are shown in Table 1. The fluorescence lifetimes (τ), radiative decay rates (k_r), and non-radiative decay rates (k_{nr}) of these compounds in $CHCl_3$, THF, DMF, these solid states, and cast films are shown in Table 2.

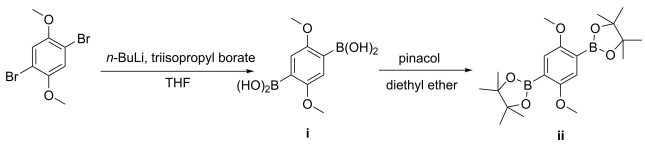

Scheme 1. Synthesis of 2,5-dimethoxy-1,4-benzenedibronic acid bis(pinacol)ester (**ii**).

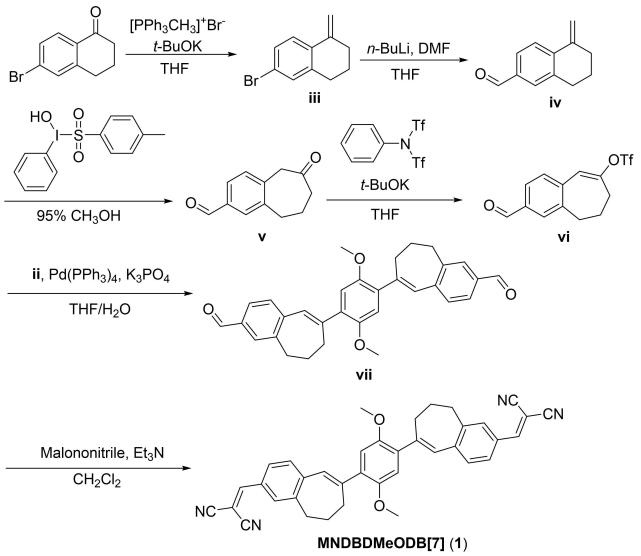

Scheme 2. Synthesis of **MNDBDMeODB[7]** (**1**).

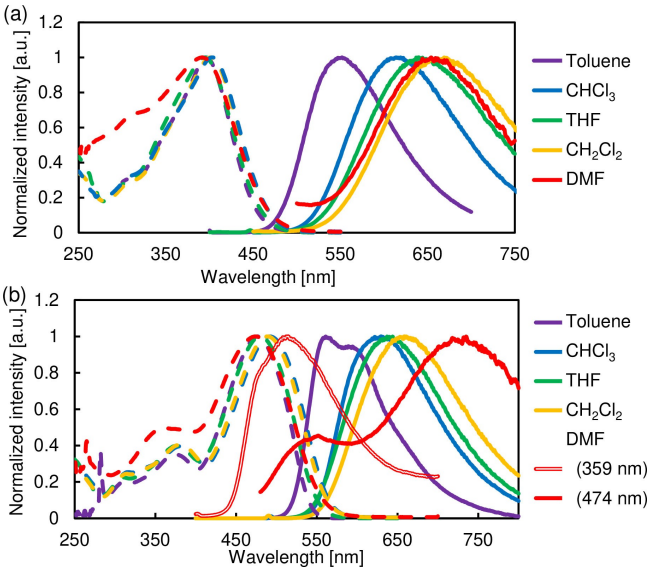

Figure 2. Absorbance (dashed line) and fluorescence (solid line) spectra of (a) **1** and (b) **2** in various solvents.

1 has a unimodal peak with a maximal absorption wavelength (λ_{abs}) of approximately 400 nm in each solvent investigated (Figure 2a). Moreover, its molar absorption coefficients (ε) are approximately 45000 $M^{-1}cm^{-1}$ in $CHCl_3$, THF, and CH_2Cl_2, and 32000 $M^{-1}cm^{-1}$ in DMF. The absorption spectrum of **1** exhibited a shoulder at approximately 300 nm only in DMF. An accurate ε could not be measured in toluene owing to the poor solubility of the compound. The λ_{fl} of **1** red-shifted with increasing solvent polarity from 552 nm in toluene to 660 nm in CH_2Cl_2. The Φ of **1** in toluene and $CHCl_3$ are 0.171 and 0.224, respectively; however, in other solvents, they are less than 0.05. **1** possesses one τ component in $CHCl_3$ and THF, and its τ and k_r in THF are less than half those in $CHCl_3$. Meanwhile, **2** and **3** exhibited maximum local absorption at approximately 370 and 480 nm, respectively, and small shoulders at approximately

Table 1. Photophysical properties of **1**, **2**, and **3** in various solvents (1.0×10^{-5} M), these solid states, and these 0.1 wt.% doped PMMA ($M_n = 100$ k) cast films.

State	Δf	1					2					3[a]			
		ε [M^{-1} cm^{-1}]	λ_{abs} [nm]	λ_{fl}[b] [nm]	Φ[b] [–]	$\Delta\tilde{\nu}$ [cm^{-1}]	ε [M^{-1} cm^{-1}]	λ_{abs} [nm]	λ_{fl}[c] [nm]	Φ (λ_{ex})[c] [–]	$\Delta\tilde{\nu}$ [cm^{-1}]	λ_{abs} [nm]	λ_{fl}[c] [nm]	Φ (λ_{ex})[c] [–]
Toluene	0.012	–[f]	396	552	0.171	7100	23000	375	561, 589	0.777 (375 nm)	3100	373	558, 582	0.920 (373 nm)
							66000	477		0.810 (477 nm)		472		0.864 (472 nm)
$CHCl_3$	0.148	45000	403	614	0.224	8500	27000	382	630	0.740 (382 nm)	4500	373	622	0.752 (373 nm)
							68000	492		0.773 (492 nm)		483		0.799 (483 nm)
THF	0.210	47000	394	637	0.044	9700	27000	376	637	0.706 (376 nm)	5100	374	637	0.820 (374 nm)
							68000	480		0.702 (480 nm)		474		0.766 (474 nm)
CH_2Cl_2	0.217	43000	400	660	0.033	9800	28000	380	661	0.590 (380 nm)	5300	370	644	0.732 (370 nm)
							69000	489		0.616 (489 nm)		479		0.711 (479 nm)
DMF	0.274	32000	392	654	0.011	10200	–[f]	359	514	0.096 (359 nm)	7500	358	530	0.073 (358 nm)
								474	552, 735	0.033 (474 nm)		466	554, 674	0.052 (466 nm)
Solid	–	–	-	608[d]	0.418[d]	–	–	–	708[e]	0.258[e]	–	–	–	<0.01
Cast film	–	–	396	534	0.530	–	–	371	582	0.743 (371 nm)	–	475	575	0.765
								478		0.796 (478 nm)				

[a] ε could not be measured accurately due to its poor solubility, and $\Delta\tilde{\nu}$ are similar to **2** except for in DMF; thus, they are omitted. [b] Excited at λ_{abs}, [c] at each absorption peak, [d] at 450 nm, and [e] at 560 nm. [f] They could not be measured accurately due to their poor solubility.

Table 2. Fluorescence lifetimes (τ) and radiative/non-radiative (k_r/k_{nr}) rates of **1**, **2**, and **3** in various states.

Entry	State	λ_{ex} [nm]	τ_1 [ns]	τ_2 [ns]	k_{r1} [10^8 s^{-1}]	k_{r2} [10^8 s^{-1}]	k_{nr1} [10^8 s^{-1}]	k_{nr2} [10^8 s^{-1}]
1	$CHCl_3$	41	0.98	–	2.29	–	7.93	–
	THF	401	0.36	–	1.01	–	22.03	–
	DMF[a]	–	–	–	–	–	–	–
	Solid	444	0.58 (0.07)	2.56 (0.93)	7.41	1.68	9.83	2.23
	Cast film	401	0.87 (0.24)	2.52 (0.76)	6.09	2.10	5.40	1.87
2	$CHCl_3$	379	2.10	–	3.52	–	1.24	–
		510	2.18	–	3.55	–	1.04	–
	THF	379	2.30	–	3.07	–	1.28	–
		510	2.35	–	2.99	–	1.27	–
	DMF	379	0.56 (0.12)	1.97 (0.88)	1.71	0.49	16.14	4.59
		510	0.17 (0.08)	1.83 (0.92)	1.88	0.18	56.94	5.29
	Solid	510	3.36 (0.20)	7.65 (0.80)	0.77	0.34	2.21	0.97
	Cast film	379	2.11	–	3.52	–	1.22	–
		510	2.26	–	3.52	–	0.90	–
3	$CHCl_3$	379	2.06	–	3.65	–	1.20	–
		510	2.07	–	3.86	–	0.97	–
	THF	379	2.31	–	3.55	–	0.78	–
		510	2.33	–	3.29	–	1.00	–
	DMF	379	0.53 (0.15)	2.06 (0.85)	1.38	0.35	17.49	4.50
		510	0.18 (0.19)	1.60 (0.82)	2.28	0.27	53.28	5.99
	Solid[b]	–	–	–	–	–	–	–
	Cast film	510	2.31	–	3.31	–	1.02	–

[a] Not measured accurately due to its low Φ and the resolution; the resolution of the excitation laser is >0.2 ns; however, one of the lifetime components is below 0.2 ns. [b] No fluorescence.

300 nm in all solvents investigated (Figure 2b). The ε values of **2** in all solvents except DMF are 27000 (excited at ~380 nm) and 68000 $M^{-1}cm^{-1}$ (excited at ~485 nm). The ε of **2** in DMF and **3** in all solvents could not be measured because of their poor solubility. The fluorescence spectra of the two absorption peaks of **2** overlap in all solvents except DMF (Figure S2), with Φ greater than 0.59. In DMF, **2** shows different fluorescence spectra, with Φ less than 0.10. The same trend was observed for **3** (Figure S1, S3).

The τ of **2** and **3** shows a single component in $CHCl_3$ and THF and two components in DMF. In $CHCl_3$, the k_r values of **2** excited at 379 and 510 nm were nearly identical at 3.52×10^8 and 3.55×10^8 s^{-1}, respectively. The k_r of **2** in THF and **3** in $CHCl_3$ and THF showed the same trend. However, compared with those in other solvents, the major components of τ in DMF were approximately $1/10^{th}$ the value of k_r.

Previously, Li et al. reported the photophysical properties of **3** in toluene, $CHCl_3$, ethyl acetate, acetone, and acetonitrile.[22] In the π-conjugated system of **3**, electron delocalization and strong intramolecular charge transfer (ICT) effects occur via the push-pull system, and the local maximum absorptions observed at approximately 370 and 480 nm are derived from the π–π* transition and ICT effect, respectively. By contrast, the fluorescence spectra of **3** in solvents other than DMF exhibited only ICT bands and positive solvatochromism. The τ of **3** in THF and $CHCl_3$ has only one component. Moreover, local excited (LE) band fluorescence was observed at 400–500 nm when **3** was excited at 300 nm in the solvents (Figure S4). However, this fluorescence intensity is less than 3% of the ICT band, except in DMF. Therefore, internal conversion from the LE state to the ICT state occurs promptly in **3** in solvents other than DMF; consequently, the fluorescence spectra of the two absorption peaks of this compound are similar. The same explanation can be given for **2**. However, differences in the fluorescence spectra and lifetime components show that the photophysical behaviors of **2** in DMF is clearly different from that in other solvents.

To obtain a more detailed discussion of the fluorescence properties of **2** in DMF, we measured the excitation spectra at its local maximum fluorescence (Figure S5). The excitation spectra at $\lambda_{fl}=514$ and 552 nm show the same shape. The local maxima are located at 344 and 416 nm. The excitation spectrum at $\lambda_{fl}=735$ nm has a maximum at 478 nm, and the peak at 367 nm is the instrumental second-harmonic generation. We also performed fluorescence measurements of **2** and **3** in DMF under excitation at 510 nm (Figure S6). The compounds show only a unimodal peak at $\lambda_{fl}=732$ nm, and no peak is observed at approximately 550 nm. An excitation wavelength of 510 nm is included in the absorption band of the ICT effect; therefore, this fluorescence peak is the ICT band. Hence, the λ_{fl} of **2** at 514 and 552 nm are the LE bands, and that at 735 nm is the ICT band. The excitation wavelengths of the ICT band cause the LE band to shift, and the difference in the longer λ_{fl} between **2** and **3** is due to the overlap of the LE and ICT bands. These facts suggest that the rate of internal conversion from the LE to the ICT state is slower than the rate of radiative decay from the LE

state in DMF, unlike in other solvents. This phenomenon may be attributed to the high viscosity of DMF.

1 has only one absorption peak, unlike unbridged **2** and **3**, because of the overlap of two absorption peaks from the π–π* and ICT transitions via bridging. In fact, calculations using time-dependent density functional theory (TD-DFT) at the ωB97XD/6-311G(d,p) level reveal that the trend of the absorption spectra of **1** and **3** in THF is similar to that observed in the experimental spectra (Figure S22).[23] Furthermore, no correlation between ε and solvent polarity is observed, thus suggesting that the conformational change is not caused by permittivity. **1** has positive solvatochromism owing to excited ICT, similar to **2** and **3**. We compared the fluorescent solvatochromic properties of **1** and **2** using the Lippert-Mataga equations[24] (1) and (2), which are defined as follows (Table 1):

$$\Delta f = \frac{\varepsilon - 1}{2\varepsilon + 1} - \frac{n^2 - 1}{2n^2 + 1} \quad (1)$$

$$\Delta\tilde{\nu} = \tilde{\nu}_a - \tilde{\nu}_e = \frac{2(\mu_e - \mu_g)^2}{4\pi\varepsilon_0 hca^3}\Delta f + \text{constant} \quad (2)$$

where Δf is a polar parameter, $\Delta\tilde{\nu}$ is the Stokes shift (cm^{-1}), and $\tilde{\nu}_a$ and $\tilde{\nu}_e$ are the wavenumbers of λ_{abs} and λ_{fl}, respectively. The Lippert-Mataga plots of **1** and **2** in each solvent show good linearity (Figure 3). **1** and **2** exhibit similar λ_{fl} in THF and CH_2Cl_2, which suggests that the luminescent species in their excited states in highly polar solvents are ICT complexes with the same electronic states. However, the λ_{fl} values of **1** in toluene and $CHCl_3$ were approximately 10 nm more red-shifted than those of **2**. In addition, the k_r and k_{nr} of **1** revealed more rapid changes in THF and $CHCl_3$ compared with those of **2** and **3**. Therefore, the ICT states of **1** differ from those of **2** in their excited states in low-polarity solvents. Moreover, the rapid decrease in Φ between low- and high-polarity solvents is observed in **1** but not in **2** and **3**. The Φ of **1** in solvents more polar than THF is less than that of **2** with longer wavelength emission in the same solvents. Therefore, the accessibility of the CI, rather than the energy gap law, reduces the Φ of **1** to less than 0.05 via flexible bridging for the vinylene groups, similar to our 8-([1,1′-biphenyl]-4-yl)-6,7-dihydro-5H-benzo[7]annulene; (bridged-phenylstilbene: **BPST[7]**)[13] and **DBDB[7]**[7] (Figure 1). In general, the dipole moments of push-pull dyes interact strongly with solvents as the solvent polarity increases, and the ICT state in the excited states changes significantly.[25] Consequently, large alternations in λ_{fl} are often observed in solvents. In addition, the emission behavior of **1** differs from that in the twisted ICT (TICT) state, where the λ_{fl} are extremely red-shifted, and the energy gap law is violated, as noted above. These phenomena change the accessibility of the CI. Similar characteristics have been previously reported for wavelengths shorter than that of **1**.[26] However, the relationship between solvent polarity and the CI is not often discussed because of the many complex factors involved in the photophysical process of push-pull type AIEgens. In addition, quantum calculations of the excited states, especially the CI, are extremely challenging for molecules as large as **1**. Therefore, this study only describes these possibilities. Both **1** and **2** have a large $\Delta\tilde{\nu}$. In particular, the absorption and fluorescence spectra of **1** hardly overlap. A large $\Delta\tilde{\nu}$ is useful for various applications because it inhibits molecular self-absorption.

Next, the photophysical properties of the target compounds in the solid-state and PMMA cast films are discussed. In the solid state, **1** exhibits strong red-orange emission (λ_{fl} = 608 nm, Φ = 0.418) with τ_1 = 0.58 ns (7%) and τ_2 = 2.56 ns (93%), while **2** emits a red color (λ_{fl} = 708 nm, Φ = 0.258) with τ_1 = 3.36 ns (20%) and τ_2 = 7.65 ns (80%) (Figure 4). However, **3** showed almost no emission in the solid state. In the PMMA cast films, **1** exhibited the shortest λ_{fl} (534 nm) with Φ = 0.530 in all states, whereas **2** and **3** showed the same λ_{fl} and Φ observed in toluene as well as structureless emission bands (Figure 4b, S7).

Gierschner reported that **DSB** forms pronounced H-aggregates with long lifetimes and fast exciton migration, and the exciton is mainly trapped by polarons, structural dislocations, triplets, and impurities; thus, intrinsically polycrystalline samples of H-aggregates with highly bright emission are difficult to achieve.[27] Therefore, the fluorescence quenching of **3** via intermolecular electronic interactions is due to its good packing and formation of strong H-aggregates in the solid state. By contrast, disruption of the molecular packing by ethylhexyl

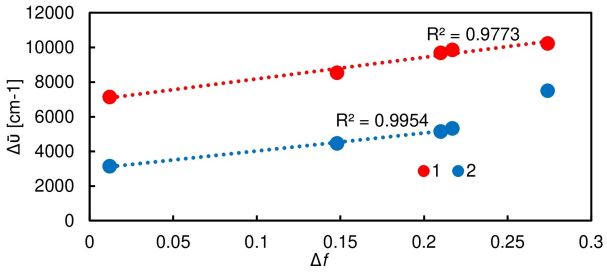

Figure 3. Lippert-Mataga plot of **1** and **2**.

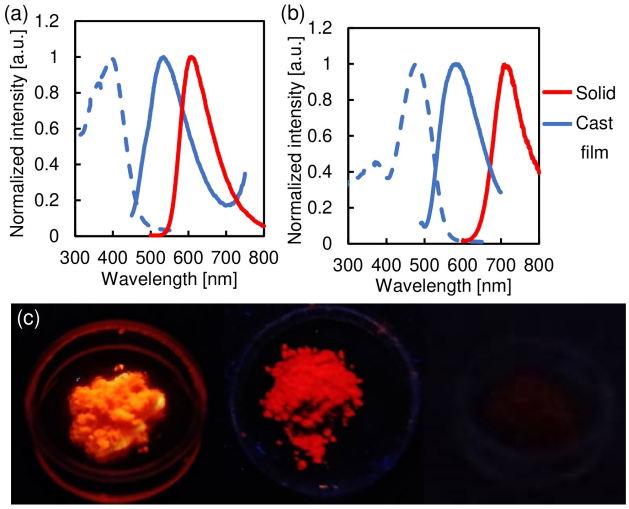

Figure 4. Absorption (dashed line) and fluorescence (solid line) of (a) **1** and (b) **2**, and (c) fluorescence images of **1**, **2**, and **3** (left to right) in their solid states.

groups or bridging suppresses the formation of H-aggregates; thus, **1** and **2** show notable emissions. **1** had a higher Φ in the solid state than in the solvents and exhibited AIE properties in solvents more polar than THF and the solid state imply that an intermolecular electronic interaction occurs in the solid state, which is different from that observed in **DBDB[7]**. However, the flexible bridges of the molecule adopt an alignment with enhanced radiative decay, such as J-aggregates,[28] or suppress quenching via intermolecular electronic interactions; as a result, the Φ of **1** in the solid state is higher than that in the solvents. Although **2** emits a red color, it is 100 nm red-shifted compared with the emission of **1**. The numbers of the lifetime components of **2** in THF and the solid state are different, similar to **1**. Thus, intermolecular electronic interactions also occur in **2** in the solid state. Previous reports indicated that **DSB** and ((1E,1′E)-(2,5-dimethyl-1,4-phenylene)bis(ethene-2,1-diyl))dibenzene (distyryldimethylbenzene: **DSDMB**), which have two methyl groups substituted into the central benzene of **DSB** (Figure 1), exhibit longer λ_{fl} in the solid state than in THF because of their highly planar conformations despite the occurrence of intermolecular electronic interactions in the solid state (**DSDMB**: $\lambda_{fl,\ THF} = 426$ nm, $\lambda_{fl,\ solid} = 451$ nm).[7,29] On the other hand, **DBDB[7]** and 8,8′-(2,5-dimethyl-1,4-phenylene)bis(6,7-dihydro-5H-benzo[7]annulene) (di-bridged **DSDMB**; **DBDMDB[7]**, Figure 1) form twisted bridged C=C or twisted C–C bonds combining bridged C=C and central benzene rings in the solid state, and show similar λ_{fl} in the solid state and THF (**DBDMDB[7]**: $\lambda_{fl,\ THF} = 392$ nm, $\lambda_{fl,\ solid} = 382$ nm).[7] The same change in the photophysical properties of **2** and **DSDMB** in THF and the solid state suggests that the molecular structure of **2** in the solid state is highly planar. Because the λ_{abs} of **1** is shorter than that of **2** in the solvents and PMMA cast films, **1** is likely to form a twisted C–C conformation, similar to **DBDMDB[7]**. Therefore, differences in conformation considerably affect the λ_{fl} of **1** and **2**. **2** realizes red emission owing to its extended π-conjugation by forming a planar conformation. The single-crystal X-ray structural analysis of **1** and **2** could not be performed; thus, we calculated the optimized structure of **1** *in vacuo* using DFT at the ωB97XD/6-311G(d,p) level of theory.[23] The results showed that the C–C bonds connecting the bridged C=C bonds and central benzene rings of **1** are twisted (Figure S23a). The planar conformation of the optimized structure of **3** is shown Figure S23b, and **2** is expected to form a conformation similar to that of **3**.

2 shows a significant difference in Φ and λ_{fl} between the solid and thin-film forms. When a film was prepared using dilute $CHCl_3$ solutions of the dye and PMMA, the crystallinity of the dye was lower than that of the polycrystalline solid obtained by recrystallization. In the thin film, the intermolecular distance between two molecules of **2** is longer than that in the polycrystalline solid, and its intermolecular electronic interactions are greatly suppressed. In other words, **2** forms H-aggregates like **3** more hardly in the thin film than in the solid state. This consequently leads to the significant difference in the Φ and $\lambda_{fl.}$ **1** also shows a difference in the Φ and λ_{fl} between the solid and thin-film forms; however, the difference is smaller than that of **2**, implying that the intermolecular electronic interactions of **2** are stronger than those of **1** in the solid state.

For further discussion, 2,2′-(((2,5-di-tert-butoxy-1,4-phenylene)-bis(6,7-dihydro-5H-benzo[7]annulene-8,3-diyl))bis(methaneylylidene))dimalononitrile (**MNDBD^{t}BuODB[7]**) (**4**), in which *tert*-butoxy groups replace the methoxy groups of **1**, was synthesized and its photophysical properties were measured in THF, the solid state, and a 0.1 wt.% doped PMMA cast film (Table 3). In THF, the photophysical properties of **4** are slightly different from those of **1**. However, in the solid state, **4** shows a 37 nm blue-shifted λ_{fl} and its Φ was 0.211 smaller than that of **1**. Furthermore, even in the PMMA cast film, **4** exhibits a 13 nm blue-shifted λ_{fl} with a shoulder at approximately 480 nm, and its Φ is 0.208 smaller than that of **1**.

The change in the crystalline system assumes a large influence on λ_{fl} and Φ if the strong crystalline fluorescence of **1** is derived from crystalline systems that improve the radiation rate, such as J-aggregates. The substituent size of **4** with *tert*-butoxy groups is larger than that of **1** with methoxy groups. Thus, the photophysical properties of **4** may be attributed to several aspects. One possibility is that the disordering of the ideal J-aggregate packing by *tert*-butoxy groups may reduce the λ_{fl} and Φ of **4** relative to those of **1**. Another possibility is that the long distance between chromophores generally reduces intermolecular electronic interactions and avoids concentration quenching, which tends to result in a high Φ. In fact, **1**, **2**, and **3** show stronger emissions in PMMA cast films than in the solid state. **4** has a smaller Φ than **1** in the solid state and PMMA cast film; however, bulky substituents are expected to increase the distance between chromophores. In **DBDB[7]**s, the introduction of bulky *tert*-butyl groups alters the molecular conformation in the solid state and decreases Φ.[7] Therefore, molecular conformational changes are also possible in **4**.

The following section discusses whether **1** forms J-aggregates. We performed an aggregation experiment of **1** in a THF/water mixed solvent (Table S1, Figure 7, S17–20) to consider the luminescence mode of **1** in the solid state. In 10–40% water suspensions, no significant changes in the absorption spectra of **1** and almost no emissions are observed. In the 50% water suspension, ε decreases by 10000 $M^{-1}cm^{-1}$ compared with that in THF. In the 60–80% water suspension, **1** has four absorption peaks, and in the 90% water suspension, the absorption peak is 384 nm and has a much broader band (Figure 5). In suspensions

Table 3. Photophysical properties of **4** in dilute THF and this solid state.

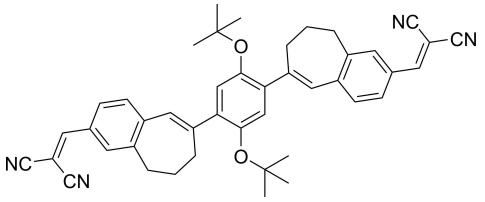

State	ε [M^{-1} cm^{-1}]	λ_{abs} [nm]	λ_{fl} [nm]	Φ [–]
THF	55000	396	652	0.014
Solid	–	–	571	0.207
Cast film	–	397	521	0.322

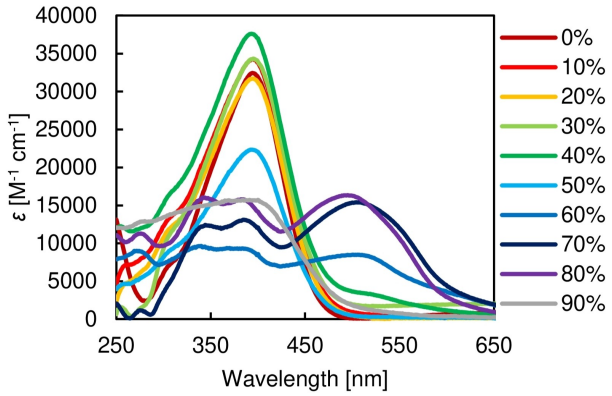

Figure 5. Absorption spectra of **1** in THF/water mixed solvent. % shows water fraction.

containing over 60% water, λ_{fl} is 601–622 nm for most of the absorption peaks, with Φ close to 0.100 or greater.

The changes in the absorption spectra indicate that **1** forms aggregates in suspensions containing over 60% water. J-aggregates have red-shifted, sharper absorption peaks compared with the absorption peak in solution because of the one-dimensional binding of dyes. The absorption peaks and Φ of J-aggregates continuously increase, and their fluorescence spectra gradually red-shift as the degree of dye aggregation increases. The aggregates of **1** exhibit more red-shifted absorption peaks in the mixed solvent than in THF; however, the peaks are broad and do not change continuously. In addition, Φ is smaller in the 80% suspension than in the 60% suspension, and λ_{fl} is almost constant. Thus, we can assume that **1** does not form J-aggregates because aggregates of **1** exhibit an emission behavior different from that of typical J-aggregates. These results suggest that **1** has strong emissions owing to the suppression of intermolecular electronic interactions in the solid state via bridging, and that the difference in fluorescence characteristics between **1** and **4** is due to the difference in their molecular conformations. The basic skeleton, **3**, shows no emission in the solid state. However, emission in the solid state is possible by collapsing the molecular packing through the introduction of bridging or ethylhexyl groups. **1** is an AIEgen that can be used in solvents more polar than THF and exhibits strong red-orange fluorescence in the solid state. Thus, **1** has potential applications in the medical field because long-wavelength luminescence is less harmful to living organisms. By contrast, **2** emits light in the near-infrared region in the solid state. Few organic light-emitting dyes with such colors are available. Therefore, **2** may potentially be used for red-light-emitting materials. In addition, substituents such as *tert*-butoxy groups can control molecular conformations. The dyes emit light of different colors.

Conclusion

We developed a red-orange light-emitting AIEgen, **MNDBDMeODB[7]** (**1**). **1** shows red-orange solid-state emission with $\lambda_{fl}=608$ nm and $\Phi=0.418$. **MNDSDMeOB** (**3**), with the bridging structure removed from **1**, exhibited positive solvatochromism in solution and no fluorescence in the solid state owing to its high crystallinity and strong intermolecular electronic interaction. The bridging structure improved the accessibility of the CI in solution and imparted AIE properties to **1**, especially in highly polar solvents. The introduction of the bridging structure into the vinylene group is a powerful strategy for the design of AIEgens. **MNDSD(EHO)B** (**2**), in which the methoxy groups of **3** are replaced with disordered ethylhexyloxy groups, showed red fluorescence with $\lambda_{fl}=708$ nm and $\Phi=0.258$ in the solid state, in addition to solvatochromic properties similar to those of **3** in solution. Only by introducing a bridging structure were red-emitting AIE-type **DSB** derivatives achieved. **1** and **2** has $\Delta\tilde{\nu}$ in both solution and the solid states that are so large that their absorption and fluorescence spectra do not overlap. A large $\Delta\tilde{\nu}$ is an important factor in the design of light-emitting devices and materials because it decreases self-absorption. In addition, **1** and **2** emit colors in PMMA cast films that are significantly different from those observed in the solid state, thus suggesting that multiple fluorescent colors can be obtained with appropriate processing. **DSB** derivatives with fluorescence properties, such as **1** and **2**, have not been previously reported. Dyes with the same main skeleton show reduced topological defects during mixing and may be highly applicable to multicolor devices/materials if their fluorescence colors can be freely tuned. Obtaining red to near-infrared emission is advantageous for biological tissue permeability and noninvasiveness. Overall, this study can potentially improve the functionality of devices and materials using the **DSB** framework. In future work, we will replace the methoxy groups of **1** with stronger donor groups, such as dialkylamino groups, to obtain an AIEgen with red/near infrared emission in the solid state.

Experimental Section

Synthesis of MNDBDMeODB[7][30]

Synthesis of 2,5-dimethoxy-1,4-benzenediboronic acid (i)[30a]

1,4-Dibromo-2,5-dimethoxybenzene (1.40 g, 4.7 mmol) was dissolved in THF (30 mL) under an argon atmosphere and cooled to −78 °C. Next, 2.6 M *n*-BuLi in hexane (3.82 mL) was dropped into the solution over 15 min, and the mixture was stirred at −78 °C for 5 h. Then, triisopropyl borate (4.77 mL, 20.8 mmol) was added to the mixture, which was subsequently stirred at −78 °C overnight. The mixture was added with 5% aqueous HCl and evaporated under reduced pressure. The residue was filtered, washed three times with water, and dried in a dryer to give crude **i** as a colorless solid. Yield: 53%; ^{1}H NMR (500 MHz, DMSO–D6) δ 7.79 (s, 4H), 7.16 (s, 2H), 3.77 (s, 6H) (Figure S24).

Synthesis of 2,5-dimethoxy-1,4-benzenediboronic acid bis(pinacol)ester (ii)[30b]

i (0.45 g, 2.0 mmol) and pinacol (0.52 g, 4.4 mmol) were dissolved in diethyl ether (15 mL). The reaction mixture was stirred at room temperature for 20 h and then evaporated under reduced pressure. The residue was extracted with CH_2Cl_2, and the organic layer was washed three times with water, dried over $MgSO_4$, filtered, and evaporated under reduced pressure to give crude **ii** as a colorless solid. Yield: 94%; ^{1}H NMR (500 MHz, $CDCl_3$) δ 7.15 (s, 2H), 3.82 (s, 6H), 1.35 (s, 24H) (Figure S25).

Synthesis of 6-bromo-1-methylene-1,2,3,4-tetrahydronaphthalene (iii)[30c]

Methyltriphenylphosphonium bromide (5.36 g, 15.0 mmol) was dissolved in THF (30 mL) under an argon atmosphere and cooled to 0 °C. Potassium *tert*-butoxide (1.68 g, 15.0 mmol) and 6-bromo-1-tetralone (2.25 g, 10.0 mmol) were added to the solution, and the reaction mixture was stirred at room temperature for 2 h. Saturated aqueous NH_4Cl was added to the mixture, which was subsequently extracted with ethyl acetate. The organic layer was washed with three times with water, dried over $MgSO_4$, filtered, and evaporated under reduced pressure. The residue was chromatographed over silica gel by eluting with hexane to give crude **v** as a colorless oil. Yield: 93.2%; ^{1}H NMR (399 MHz, $CDCl_3$) δ 7.49 (dd, J = 5.5, 3.7 Hz, 1H), 7.27–7.25 (m, 2H), 5.46 (s, 1H), 4.97 (s, 1H), 2.81 (t, J = 6.2 Hz, 2H), 2.54–2.51 (m, 2H), 1.89–1.83 (m, 2H) (Figure S26).

Synthesis of 5-methylene-5,6,7,8-tetrahydronaphthalene-2-carbaldehyde (iv)

iii (2.08 g, 9.32 mmol) was dissolved in dry THF under an argon atmosphere and cooled to −78 °C. Next, 2.6 M *n*-BuLi in hexane (3.94 mL) was dropped into the solution over 15 min, and the mixture was stirred at −78 °C for 30 min. Then, DMF (0.85 mL, 10.2 mmol) was added to the mixture, which was subsequently stirred at room temperature for 1.5 h. Saturated aqueous NH_4Cl was added, and the mixture was extracted with ethyl acetate. The organic layer was washed three times with water, dried over $MgSO_4$, filtered, and evaporated under reduced pressure. The residue was chromatographed over silica gel by eluting with hexane/ethyl acetate (4:1, v/v) to give crude **iv** as a yellow oil. Yield: 87%; ^{1}H NMR (500 MHz, $CDCl_3$) δ 9.95 (s, 1H), 7.78 (d, J = 8.2 Hz, 1H), 7.65 (d, J = 8.2 Hz, 1H), 7.61 (s, 1H), 5.63 (s, 1H), 5.13 (s, 1H), 2.92 (t, J = 6.3 Hz, 2H), 2.58 (t, J = 5.8 Hz, 2H), 1.93–1.88 (m, 2H) (Figure S27).

Synthesis of 6-oxo-6,7,8,9-tetrahydro-5H-benzo[7]annulene-2-carbaldehyde (v)[30d]

iv (1.39 gm, 8.1 mmol) was dissolved in 95% CH_3OH (40 mL). [Hydroxy(tosyloxy)iodo]benzene (3.17 g, 8.1 mmol) was added to the mixture, which was subsequently stirred at room temperature for 20 min. Water was added, and the mixture was extracted with CH_2Cl_2. The organic layer was washed three times with water, dried over $MgSO_4$, filtered, and evaporated under reduced pressure. The residue was chromatographed over silica gel by eluting with hexane/ethyl acetate (3:1, v/v) to give crude **v** as a yellow oil. Yield: 81%; ^{1}H NMR (500 MHz, $CDCl_3$) δ 9.98 (s, 1H), 7.70 (d, J = 7.9 Hz, 2H), 7.33 (d, J = 7.6 Hz, 1H), 3.81 (s, 2H), 3.05 (t, J = 6.3 Hz, 2H), 2.60 (t, J = 6.9 Hz, 2H), 2.06–2.01 (m, 2H) (Figure S28).

Synthesis of 3-formyl-6,7-dihydro-5H-benzo[7]annulen-8-yl trifluoromethanesulfonate (vi)[30e]

v (1.23 g, 6.5 mmol) was dissolved in THF (20 mL) under an argon atmosphere and cooled to −20 °C. Potassium *tert*-butoxide (0.81 g, 7.2 mmol) was added to the solution, and the reaction mixture was stirred at 0 °C for 1 h and then cooled to −20 °C. *N*-Phenylbis(trifluoromethanesulfonimide) (2.58 g, 7.2 mmol) was added to the mixture, which was subsequently stirred at −20 °C for 1 h and then at 0 °C for 4 h. Water was added, and the mixture was extracted with ethyl acetate. The organic layer was washed three times with water, dried over $MgSO_4$, filtered, and evaporated under reduced pressure. The residue was chromatographed over silica gel by eluting with hexane/ethyl acetate (6:1, v/v) to give crude **viii** as a yellow oil. Yield: 78%; ^{1}H NMR (500 MHz, $CDCl_3$) δ 9.98 (s, 1H), 7.71 (d, J = 7.9 Hz, 1H), 7.63 (s, 1H), 7.34 (d, J = 7.6 Hz, 1H), 6.65 (s, 1H), 2.98 (t, J = 5.0 Hz, 2H), 2.83 (t, J = 6.6 Hz, 2H), 2.05–2.01 (m, 2H) (Figure S29).

Synthesis of 8,8′-(2,5-dimethoxy-1,4-phenylene)bis(6,7-dihydro-5H-benzo[7]annulene-3-carbaldehyde) (vii)[30f]

vi (0.67 g, 2.1 mmol), **ii** (0.32 g, 0.8 mmol), $Pd(PPh_3)_4$ (0.03 g, 0.03 mmol), and K_3PO_4 (0.53 g, 2.5 mmol) were dissolved in THF/water (15 mL; 5:1, v/v) under an argon atmosphere and stirred at 30 °C for 24 h. Water was added, and the mixture was extracted with CH_2Cl_2. The organic layer was washed three times with water, dried over $MgSO_4$, filtered, and evaporated under reduced pressure. The residue was chromatographed over silica gel by eluting with CH_2Cl_2 to give crude **vii** as a yellow solid. Yield: >99%; ^{1}H NMR (500 MHz, $CDCl_3$) δ 9.98 (s, 2H), 7.70 (d, J = 6.7 Hz, 4H), 7.33 (d, J = 7.9 Hz, 2H), 6.86 (s, 2H), 6.66 (s, 2H), 3.85 (s, 6H), 2.95 (t, J = 6.1 Hz, 4H), 2.64 (t, J = 6.6 Hz, 4H), 2.27–2.22 (m, 4H) (Figure S30).

Synthesis of (MNDBDMeODB[7] (1)[30g]

vii (0.42 g, 0.9 mmol) was dissolved in CH_2Cl_2 (15 mL) and added with malononitrile (0.14 g, 2.2 mmol) and one portion of triethylamine. The reaction mixture was stirred overnight at room temperature in the dark and then evaporated. The residue was chromatographed over silica gel by eluting with CH_2Cl_2 and then recrystallized to give **MNDBDMeODB[7]** (**1**) as a red solid. Yield: 30%; ^{1}H NMR (500 MHz, $CDCl_3$) δ 7.77 (d, J = 9.2 Hz, 2H), 7.70 (d, J = 2.7 Hz, 4H), 7.31 (d, J = 7.9 Hz, 2H), 6.84 (s, 2H), 6.63 (s, 2H), 3.85 (s, 6H), 2.94 (t, J = 6.0 Hz, 4H), 2.68 (t, J = 6.4 Hz, 4H), 2.25–2.20 (m, 4H) (Figure S31); FTIR (KBr) 2230 cm^{-1}; HRMS (FAB) Calcd for $C_{38}H_{30}N_4O_2$: 574.2369, Found 574.2372 (Figure S43). ^{13}C NMR spectra could not be measured due to poor solubility of the compound in $CDCl_3$.

Acknowledgements

The authors thank Mr. Masato Koizumi (Materials Analysis Division, Tokyo Institute of Technology) for the HRMS measurements. The authors also thank Dr. Noritaka Sakakibara (Department of Chemistry, Tokyo Institute of Technology) for the support of fluorescence lifetime measurements. This research was supported in part by MEXT/JSPS KAKENHI grants 23H05145, 18H02045, and 17H05145 (GK), and by the Toshiaki Ogasawara Memorial Foundation (GK).

Conflict of Interests

The authors declare no conflict of interest.

Data Availability Statement

The data that support the findings of this study are available from the corresponding author upon reasonable request.

Keywords: distyrylbenzene · aggregation-induced emission · push-pull fluorophore · red-emitting fluorophore · fluorescent solvatochromism

[1] a) H. Sasabe, J. Kido, *J. Mater. Chem. C* **2013**, *1*, 1699–1707; b) N. Okada, S. Nakatsuka, R. Kawasumi, H. Gotoh, N. Yasuda, T. Hatakeyama, *Chem. Eur. J.* **2023**, *29*, e202202627; c) M. Shimizu, T. Sakurai, *Aggregate* **2022**, *3*, e144; d) C.-Y. Chan, M. Tanaka, Y.-T. Lee, Y.-W. Wong, H. Nakanotani, T. Hatakeyama, C. Adachi, *Nat. Photonics* **2021**, *15*, 203–207; e) S. Oda, W. Kumano, T. Hama, R. Kawasumi, K. Yoshiura, T. Hatakeyama, *Angew. Chem. Int. Ed.* **2021**, *60*, 2882–2886; f) J. Kashida, Y. Shoji, Y. Ikabata, H. Taka, H. Sakai, T. Hasobe, H. Nakai, T. Fukushima, *Angew. Chem. Int. Ed.* **2021**, *60*, 23812–23818; g) L. Arrico, L. D. Bari, F. Zinna, *Chem. Eur. J.* **2021**, *27*, 2920–2934; h) U. Balijapalli, R. Nagata, N. Yamada, H. Nakanotani, M. Tanaka, A. D'Aléo, V. Placide, M. Mamada, Y. Tsuchiya, C. Adachi, *Angew. Chem. Int. Ed.* **2021**, *60*, 8477–8482; i) J. Gierschner, J. Q. Shi, B. Milian-Medina, D. Roca-Sanjuan, S. Varghese, S. Park, *Adv. Opt. Mater.* **2021**, *9*, 2002251; j) G. Hong, X. Gan, C. Leonhardt, Z. Zhang, J. Sibert, J. M. Busch, S. Bräse, *Adv. Mater.* **2021**, *33*, 2005630; k) H. Arai, H. Sasabe, H. Tsuneyama, K. Kumada, J. Kido, *Chem. Eur. J.* **2021**, *27*, 10780–10780; l) I. S. Park, H. Min, T. Yasuda, *Aggregate* **2021**, *2*, e96; m) F. Ito, R. Naganawa, Y. Fujimoto, M. Takimoto, Y. Mochiduki, S. Katsumi, *ChemPhysChem* **2021**, *22*, 1662–1666; n) I. S. Park, H. Min, T. Yasuda, *Aggregate* **2021**, *2*, e96; o) H. Tsuji, *Bull. Chem. Soc. Jpn.* **2022**, *95*, 657–662; p) W. Zhang, T. Sakurai, M. Aotani, G. Watanabe, H. Yoshida, V. S. Padalkar, Y. Tsutsui, D. Sakamaki, M. Ozaki, S. Seki, *Adv. Opt. Mater.* **2019**, *7*, 1801349.

[2] a) A. S. Klymchenko, *Acc. Chem. Res.* **2023**, *56*, 1–12; b) J. Shaya, P. R. Corridon, B. Al-Omari, A. Aoudi, A. Shunnar, M. I. H. Mohideen, A. Qurashi, B. Y. Michel, A. Burger, *J. Photochem. Photobiol. C* **2022**, *52*, 100529; c) X. Cai, B. Liu, *Angew. Chem. Int. Ed.* **2020**, *59*, 9868–9886; d) G. K. Kole, M. Koscak, A. Amar, D. Majhen, K. Bozinovic, Z. Brkljaca, M. Ferger, E. Michail, S. Lorenzen, A. Friedrich, I. Krummenacher, M. Moos, H. Braunschweig, A. Boucekkine, C. Lambert, J. F. Halet, I. Piantanida, K. Muller-Buschbaum, T. B. Marder, *Chem. Eur. J.* **2022**, *28*, e202200753; B. A. D. Neto, J. R. Correa, J. Spencer, *Chem. Eur. J.* **2022**, *28*, e202103262; e) H. Li, H. Kim, J. Han, V. Nguyen, X. Peng, J. Yoon, *Aggregate* **2021**, *2*, e51; f) J. Mei, H. Tian, *Aggregate* **2021**, *2*, e32; g) B. Andreiuk, I. O. Aparin, A. Reisch, A. S. Klymchenko, *Chem. Eur. J.* **2021**, *27*, 12877–12883; h) C. Wang, M. Taki, Y. Sato, Y. Tamura, H. Yaginuma, Y. Okada, S. Yamaguchi, *Proc. Natl. Acad. Sci. USA* **2019**, *116*, 15817–15822; i) Y. Niko, P. Didier, I. Mely, G. Konishi, A. S. Klymchenko, *Sci. Rep.* **2016**, *6*, 18870; j) C. Wang, A. Fukazawa, M. Taki, Y. Sato, T. Higashiyama, S. Yamaguchi, *Angew. Chem. Int. Ed.* **2015**, *54*, 15213–15217; k) Y. Niko, Y. Arntz, Y. Mely, G. Konishi, A. S. Klymchenko, *Chem. Eur. J.* **2014**, *20*, 16473–16477; l) Y. Niko, H. Moritomo, H. Sugihara, Y. Suzuki, J. Kawamata, G. Konishi, *J. Mater. Chem. B* **2015**, *3*, 184–190.

[3] a) A. J. C. Kuehne, M. C. Gather, *Chem. Rev.* **2016**, *116*, 12823–12864; b) I. D. W. Samuel, G. A. Turnbull, *Chem. Rev.* **2007**, *107*, 1272–1295; c) D. Venkatakrishnarao, S. Hasebe, Y. Egawa, J. Tapar, R. Paniagua-Domínguez, C. S. Lau, H. Yamagishi, H. Tsuji, Y. Yamamoto, *Adv. Photonics Res.* **2023**, *4*, 2200357; d) X. Liu, M. Sang, H. Lin, C. Liu, J. Zhang, J. Yi, K. Gao, W.-Y. Lai, W. Huang, *Chem. Eur. J.* **2020**, *26*, 3103–3112; e) Y. Oyama, M. Mamada, A. Shukla, E. G. Moore, S.-C. Lo, E. B. Namdas, C. Adachi, *ACS Materials Lett.* **2020**, *2*, 161–167; f) M. Uchimura, Y. Watanabe, F. Araoka, J. Watanabe, H. Takezoe, G. Konishi, *Adv. Mater.* **2010**, *22*, 4473–4478.

[4] a) A. Abdollahi, H. Roghani-Mamaqani, B. Razavi, M. Salami-Kalajahi, *ACS Nano* **2020**, *14*, 14417–14492; b) J. I. Deneff, K. S. Butier, L. E. S. Rohwer, C. J. Pearce, N. R. Valdez, M. A. Rodriguez, T. S. Luk, D. F. S. Gallis, *Angew. Chem. Int. Ed.* **2021**, *60*, 1203–1211; c) S. Cherumukkil, G. Das, R. P. N. Triphathi, G. V. PavanKumar, S. Varughese, A. Ajayaghosh, *Adv. Funct. Mater.* **2022**, *32*, 2109041; d) A. Kalita, A. H. Malik, N. S. Sarma, *Chem. Asian J.* **2020**, *15*, 1074–1080:; e) T. Rappitsch, S. M. Borisov, *Chem. Eur. J.* **2021**, *21*, 10685–10692.

[5] a) S. W. Thomas, G. D. Joly, T. M. Swager, *Chem. Rev.* **2007**, *107*, 1339–1386; b) S. Fan, G. Zhang, G. H. Dennison, N. FitzGerald, P. L. Burn, I. R. Gentle, P. E. Shaw, *Adv. Mater.* **2020**, *32*, 1905785; c) V. Mertz, J. Mertz, M. Kirchner, J. Lenhart, T. B. Marder, A. Krueger, *Chem. Eur. J.* **2021**, *27*, 8118–8126; d) Y. Sasaki, K. Asano, T. Minamiki, Z. Zhang, S. Takizawa, R. Kubota, T. Minami, *Chem. Eur. J.* **2020**, *26*, 14525–14529; e) R. Huang, M. Li, D. Lin, Y. Shao, C. Shang, Q. Liu, N. Li, R. Miao, H. Peng, Y. Tang, Y. Tang, *Aggregate* **2023**, *4*, e203; f) L. Singh, N. Ranjan, *J. Am. Chem. Soc.* **2023**, *145*, 2745–2749.

[6] T. E. Bush, G. W. Scott, *J. Phys. Chem.* **1981**, *85*, 144–146.

[7] Y. Shimomura, K. Igawa, S. Sasaki, N. Sakakibara, R. Goseki, G. Konishi, *Chem. Eur. J.* **2022**, *28*, e202201884.

[8] F. D'Anna, S. Marullo, G. Lazzara, P. Vitale, R. Noto, *Chem. Eur. J.* **2015**, *21*, 14780–14790.

[9] J. Gierschner, S. Y. Park, *J. Mater. Chem. C.* **2013**, *1*, 5818–5832.

[10] C. J. Bhongale, C. W. Chang, C. S. Lee, E. W. G. Diau, C. S. Hsu, *J. Phys. Chem. B* **2005**, *109*, 13472–13482.

[11] a) S. J. Yoon, S. Y. Park, *J. Mater. Chem.* **2011**, *21*, 8338–8346; b) SJ. Yoon, J. H. Kim, J. W. Chung, S. Y. Park, *J. Mater. Chem.* **2011**, *21*, 18971–18973.

[12] A. M. Smith, M. C. Mancini, S. Nie, *Nat. Nanotechnol.* **2009**, *4*, 710–711.

[13] R. Iwai, S. Suzuki, S. Sasaki, A. S. Sairi, K. Igawa, T. Suenobu, K. Morokuma, G. Konishi, *Angew. Chem. Int. Ed.* **2020**, *59*, 10556–10573.

[14] a) Z. Zhao, H. Zhang, J. W. Y. Lam, B. Z. Tang, *Angew. Chem. Int. Ed.* **2020**, *59*, 9888–9907; b) J. Mei, N. L. C. Leung, R. T. K. Kwok, J. W. Y. Lam, B. Z. Tang, *Chem. Rev.* **2015**, *115*, 11718–11940; c) S. Suzuki, S. Sasaki, A. S. Sairi, R. Iwai, B. Z. Tang, G. Konishi, *Angew. Chem. Int. Ed.* **2020**, *59*, 9856–9867; d) S. Sasaki, S. Suzuki, W. M. C. Sameera, K. Igawa, K. Morokuma, G. Konishi, *J. Am. Chem. Soc.* **2016**, *138*, 8194–8206; e) N. L. Leung, N. Xie, W. Yuan, Y. Liu, Q. Wu, Q. Peng, Q. Miao, J. W. Lam, B. Z. Tang, *Chem. Eur. J.* **2014**, *20*, 15349–1535; f) L.-H. Wang, Y. Nagashima, M. Abekura, H. Uekusa, G. Konishi, K. Tanaka, *Chem. Eur. J.* **2022**, *28*, e202200064; g) H. V. Miyagishi, H. Masai, J. Terao, *Chem. Eur. J.* **2022**, *28*, e202103175; h) J. Rouillon, C. Monnereau, C. Andraud, *Chem. Eur. J.* **2021**, *27*, 8003–8007; i) S. Sasaki, K. Igawa, G. Konishi, *J. Mater. Chem. C* **2015**, *3*, 5940–5950.

[15] a) J. Luo, Z. Xie, J. W. Y. Lam, L. Cheng, H. Chen, C. Qiu, H. S. Kwok, X. Zhan, Y. Liu, D. Zhu, B. Z. Tang, *Chem. Commun.* **2001**, 1740–1741; b) Z. Zhao, J. W. Y. Lam, B. Z. Tang, *J. Mater. Chem.* **2012**, *22*, 23726–23740.

[16] G. Battistelli, A. Cantelli, G. Guidetti, J. Manzi, M. Montalti, *Wiley Interdiscip. Rev. Nanomed. Nanobiotechnol.* **2016**, *8*, 139–150.

[17] a) J. Mei, Y. Huang, H. Tian, *Appl. Matter. Interfaces.* **2018**, *10*, 12217–12261; b) D. Ding, K. Li, B. Liu, B. Z. Tang, *Acc. Chem. Res.* **2013**, *46*, 2441–2453; c) H.-P. Wang, X. Chen, Y.-L. Qi, L.-W. Huang, C.-X. Wang, D. Ding, X. Xue, *Adv. Drug Delivery Rev.* **2021**, *179*, 114028.

[18] a) J. Li, J. Wang, H. Li, N. Song, D. Wang, B. Z. Tang, *Chem. Soc. Rev.* **2020**, *49*, 1144–1172; b) W. Ma, W. Li, M. Gao, R. Liu, X. Zhao, X. Gong, *Org. Electron.* **2019**, *73*, 226–230; c) Q. Zhao, J. Z. Sun, *J. Mater. Chem. C.* **2016**, *4*, 10588–10609; d) J. Hwang, P. Nagaraju, M. J. Cho, D. H. Cho, *Aggregate* **2023**, *4*, e199.

[19] a) M. Shimizu, R. Kaki, Y. Takeda, T. Hiyama, N. Nagai, H. Yamagishi, H. Furutani, *Angew. Chem. Int. Ed.* **2012**, *51*, 4095–4099; b) M. Kim, D. R. Whang, J. Gierschner, S. Y. Park, *J. Mater. Chem. C* **2015**, *3*, 231; c) C. Li, M. Hanif, X. Li, S. Zhang, Z. Xie, L. Liu, B. Yang, S. Su, Y. Ma, *J. Mater. Chem. C* **2016**, *4*, 7478–7484.

[20] S. Varghese, S. J. Yoon, E. M. Calzado, S. Casado, P. G. Boj, M. A. Díaz-García, R. Rasel, R. Fischer, B. Milián-Medina, R. Wannemacher, S. Y. Park, J. Gierschner, *Adv. Mater.* **2012**, *24*, 6473–6478.

[21] a) J. Saltiel, A. S. Waller, D. F. Sears Jr, *J. Photochem. Photobiol. A* **1992**, *65*, 29–40; b) T. Tahara, H. Hamaguchi, *Chem. Phys. Lett.* **1994**, *217*, 369–374; c) T. Nakamura, S. Takeuchi, N. Suzuki, T. Tahara, *Chem. Phys. Lett.* **2008**, *465*, 212–215.

[22] J. Lv, X. Yin, H. Zheng, Y. Li, Y. Li, D. Zhu, *Luminescence* **2011**, *26*, 185–190.

[23] Gaussian 09, Revision D.01, M. J. Frisch, G. W. Trucks, H. B. Schlegel, G. E. Scuseria, M. A. Robb, J. R. Cheeseman, G. Scalmani, V. Barone, B. Mennucci, G. A. Petersson, H. Nakatsuji, M. Caricato, X. Li, H. P. Hratchian, A. F. Izmaylov, J. Bloino, G. Zheng, J. L. Sonnenberg, M. Hada, M. Ehara, K. Toyota, R. Fukuda, J. Hasegawa, M. Ishida, T. Nakajima, Y. Honda, O. Kitao, H. Nakai, T. Vreven, J. A. Montgomery, Jr., J. E. Peralta, F. Ogliaro, M. Bearpark, J. J. Heyd, E. Brothers, K. N. Kudin, V. N.

Staroverov, T. Keith, R. Kobayashi, J. Normand, K. Raghavachari, A. Rendell, J. C. Burant, S. S. Iyengar, J. Tomasi, M. Cossi, N. Rega, J. M. Millam, M. Klene, J. E. Knox, J. B. Cross, V. Bakken, C. Adamo, J. Jaramillo, R. Gomperts, R. E. Stratmann, O. Yazyev, A. J. Austin, R. Cammi, C. Pomelli, J. W. Ochterski, R. L. Martin, K. Morokuma, V. G. Zakrzewski, G. A. Voth, P. Salvador, J. J. Dannenberg, S. Dapprich, A. D. Daniels, O. Farkas, J. B. Foresman, J. V. Ortiz, J. Cioslowski, D. J. Fox, Gaussian, Inc., Wallingford CT, 2013.

[24] a) N. Mataga, H. Chosrowjan, S. Taniguchi, *J. Photochem. Photobiol. C* **2005**, *6*, 37–79; b) N. Mataga, Y. Kaifu, M. Koizumi, *Bull. Chem. Soc. Jpn.* **1956**, ***29***, 465–470; c) V. E. Lippert, *Ber. Bunsenges. Phys. Chem.* **1957**, *61*, 962–975.

[25] a) A. S. Klymchenko, *Acc. Chem. Res.* **2017**, *50*, 366–375; b) Y. Niko, S. Kawauchi, G. Konishi, *Chem. A Eur. J.* **2013**, *19*, 9760–9765; c) D. I. Danylchuk, P. H. Jouard, A. S. Klymchenko, *J. Am. Chem. Soc.* **2021**, *143*, 912–924; d) A. Marini, A. Muñoz-Losa, A. Biancardi, B. Mennucci, B, *J. Phys. Chem. B* **2010**, *114*, 17128–17135; e) S. Sasaki, G. P. C. Drummen, G. Konishi, *J. Mater. Chem. C.* **2016**, *4*, 2731–2743; f) Y. Niko, S. Sasaki, K. Narushima, D. K. Sharma, M. Vacha, G. Konishi, *J. Org. Chem.* **2017**, *80*, 10794–10805; g) S Sasaki, Y Niko, A. S. Klymchenko, G Konishi *Tetrahedron* **2014**, *70*, 7551–7559.

[26] a) X. Y. Shen, Y. J. Wang, E. Zhao, W. Z. Yuan, Y. Liu, P. Lu, A. Qin, Y. Ma, J. Z. Sun, B. Z. Tang, *J. Phys. Chem. C* **2013**, *117*, 73340–7347. DOI: 10.1021/jp311360p; b) L. Ding, Z. Zhang, X. Li, J. Su, *Chem. Commun.* **2013**, *49*, 7319–7321; c) Y. Zhang, D. Li, Y. Li, J. Yu, *Chem. Sci.* **2014**, *5*, 2710–2716.

[27] J. Gierschner, L. Lüer, B Milián-Medina, D. Oelkrug, H.-J. Egelhaaf, *J. Phys. Chem. Lett.* **2013**, *4*, 2686–2697.

[28] a) M. Reers, T. W. Smith, L. B. Chen, *Biochemistry.* **1991**, *30*, 4480–4486; b) S. Verma, A. Chosh, A. Das, H. N. Ghosh, *Chem. Eur. J.* **2011**, *17*, 3458–3464.

[29] Z. Yang, H. J. Geise, M. Mehbod, G. Debrue, J. W. Visser, E. J. Sonneveld, L. Van't dack, R. Gijbels, *Synth. Met.* **1990**, *39*, 137–151.

[30] a) C. Wang, M. Kiltiziaki, J. A. H. MacBride, L. D. W. Samuel, *Adv. Mater.* **2000**, *12*, 217–222; b) T. Koolmeister, M. Södergern, M. Scobie, *Tetrahedron Lett.* **2002**, *43*, 5965–5968; c) V. Němec, M. Hylsová, L. Maier, J. Flegel, S. Sievers, S. Ziegler, M. Schröder, B.-T. Berger, A. Chaikuad, B. Valčíková, S. Uldrijan, S. Drápela, K. Souček, H. Waldmann, S. Knapp, K. Paruch, *Angew. Chem. Int. Ed.* **2019**, *58*, 1062–1066; d) M. R. Friedfeld, M. Shevlin, G. W. Margulieux, L.-C. Campeau, P. J. Chirik, *J. Am. Chem. Soc.* **2016**, *138*, 3314–3324; e) M. W. Justik, G. F. Koser, *Molecules* **2005**, *10*, 217–225; f) T. Ueda, H. Konishi, K. Manabe, *Org. Lett.* **2012**, *14*, 5370–5373; g) G. Bagdžiūnas, S. Stončius, E. Butkus, *Synlett* **2017**, *28*, 2790–2794; h) Y. Zhang, L. Yuan, S. Jia, X. Liu, J. Zhao, G. Yin, *Phys. Chem. Chem. Phys.* **2019**, *21*, 3218–3226.

Manuscript received: April 16, 2023
Accepted manuscript online: May 10, 2023
Version of record online: ■■, ■■

RESEARCH ARTICLE

A red-emitting aggregation-induced emission luminogen (AIEgen) is realized by introducing a bridging structure into push-pull distyrylbenzene.

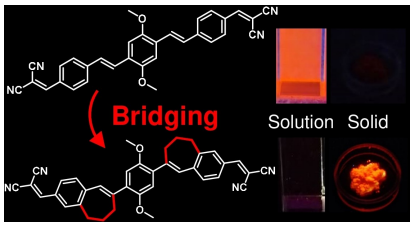

*Y. Shimomura, Prof. Dr. G.-i. Konishi**